LAWRENCE LIVERMORE NATIONAL LABORATORY

LLNL-JRNL-840584

A Multi-Modal Event Catalog and Waveform Data Set that Supports Explosion Monitoring from Nevada, USA

R. L. Rodd, R. A. Brogan, J. D. Carmichael, A. C. Price, C. J. Young

September 30, 2022

Bulletin of Seismological Society of America

LLNL-JRNL-840584

A Multi-Modal Event Catalog and Waveform Data Set that Supports Explosion Monitoring from Nevada, USA

Rebecca L. Rodd[1], Ronald A. Brogan[2], Josh D. Carmichael[3], Amanda C. Price[1], Chris J. Young[4]

[1]Corresponding Author:
Rebecca L. Rodd
Lawrence Livermore National Laboratory
700 East Ave
Livermore, CA 94550
rodd2@llnl.gov

[2]ENSCO, Inc

[3]Los Alamos National Laboratory

[4]Sandia National Laboratories

Declaration of Competing Interests

The authors acknowledge there are no conflicts of interest recorded.

Abstract

Multi-modal, curated data sets and nuisance event catalogs remain rare in the explosion monitoring community relative to curated seismic datasets. The source of this relative absence is the difficultly in deploying multi-modal receivers that sense the seismic, acoustic, and other modalities from multi-physics sources. We provide such a dataset in this study that delivers seismic, infrasound, and electromagnetic (magnetometer) sensor records collected over a two-week period, within 255km of a 10t buried chemical explosion called DAG-4 that was located at 37.1146°, -116.0693° on 22-June-2019 21:06:19.88 UTC. This catalog includes 485 seismic, seismo-acoustic, and infrasound-only events that an expert analyst manually built by reviewing waveforms from 29 seismic and infrasound sensors. Our data release includes waveforms from these 29 seismic, infrasound, and seismo-acoustic stations, two magnetometer stations, and their station metadata. We deliver these waveforms in NNSA KB Core CSS .w format (i4) with a corresponding wfdisc table that provides the header information. We expect that this dataset will provide a valuable, benchmark resource to develop signal processing algorithms and explosion monitoring methods against manual, human observations.

Introduction and Motivation

On July 16, 1945, the United States detonated the first nuclear weapon at the Trinity Site in southern New Mexico. By 1949, the Soviet Union had detonated their first device and the field of nuclear explosion monitoring was born. In the intervening decades, tremendous progress in explosion monitoring research has enabled scientists the ability to characterize nuclear explosions all over the world, and at a level that would have seemed unimaginable at the advent of monitoring. Great challenges remain, however. With improved monitoring capability, technical ambitions have grown, and the monitoring community is now focused on developing the capability needed to monitor the proposed Comprehensive Nuclear Test Ban Treaty (CTBT) that requires detection of nuclear explosions of any size, anywhere in the world (e.g., Koper 2020). Successfully monitoring the CTBT will require that detection operations exploit combinations of physical sensing modalities, which can lower monitoring thresholds over those achieved by single modalities (Carmichael et al., 2020). Unfortunately, most researchers cannot advance multi-modal monitoring techniques against ground-truth sources, largely because so few multi-modal data sets are available.

The objective of this project was to generate a multi-modal dataset to test new data processing algorithms that are being developed by the U.S. National Laboratories for improving nuclear explosion monitoring capability. It is now well-established that the far-regional/teleseismic distance verification regime implemented by the Provisional Technical Secretariat (PTS) of the Comprehensive Nuclear Test Ban Treaty Organization (CTBTO) Prepatory Committee (PrepCom) is capable of detecting fully coupled explosions of about 1 kt anywhere in the world utilizing seismic, infrasound, hydroacoustic, and radionuclide sensors (National Research

Council, 2012, Marty, 2019). The U.S. National Laboratories efforts are now focused on developing new algorithms suitable for detection and characterization of lower yield explosions recorded at local and near-regional distances (i.e. within approximately 350 km). It is our hope that by making a benchmark, multi-modal reference dataset available to the broader explosion-monitoring research community, we can involve them in the development and refinement of new data processing algorithms. We required that this dataset includes raw sensor data recorded for one ground truth explosive event, as well as a variety of background nuisance events, from local to near-regional distances. We further imposed that many sensors had legacy deployments to record historical explosions, and that we recorded such explosions and background events in a variety of sensor configurations. This particular requirement means that researchers will be able to perform data processing parametric sensitivity tests with sensor sub-networks that include capabilities unavailable to more limited single modality sensors in uniform configurations.

To meet these requirements, we collected waveform data from seismic, infrasonic, and electromagnetic sensors deployed on and around the Nevada National Security Site (NNSS) for a fifteen-day interval (June 15 to 29, 2019) centered on the June 22, 2019 DAG-4 shot, which was part of Source Physics Experiment (SPE) Phase II: Dry Alluvium Geology (DAG) (Larotonda et al., 2021). To provide information about the events that our waveform data recorded, we included an expert analyst in our data preparation. This analyst thereby manually built a comprehensive, composite catalog of seismic, infrasonic, and seismo-acoustic events during the two-week collection interval. Our analyst leveraged the available event catalogs for the region, manually revised any events that may have been mis-associated and added missing events. This paper provides a detailed summary of the content of our data set, discusses our quality control procedures and illustrates examples of multi-modal waveform records.

DAG-4 Event

There have been several explosions sourced within the NNSS over the previous 10 years that provide candidate events for multi-modality data collection against a permanent and semi-permanent network of seismic, infrasound, and electromagnetic sensors. Five such explosions were conducted through Phase I of the SPE (Snelson et al., 2013), and another four explosions were conducted through Phase II of the same series, (the DAG shots). These explosions were buried between 31m to 385m below ground surface and ranged in yield between 89 kg to 51000 kg TNT equivalent, but not all shots produced clear infrasound or electromagnetic signals. Table 1 of Blom et al. (2020) summarizes peak over-pressure records of the infrasound data. The largest and second deepest shot (DAG-2) showed no infrasound signal. The second largest shot (DAG-4) was comparatively shallow and produced visible infrasound signals that models predict are excited when the ground shock strikes ground surface and perturbs the local pressure field above the burial point (Ford et al., 2014). The chemical explosive also generated an ionizing air shock and plasma underground (Carmichael et al., 2020), which generated electromagnetic signals that appeared at multiple sensors at the expected (speed of light) arrival time. Moreover, logistical complexities associated with sensor deployment and telemetry that were present for the earlier SPE shots had been solved during recording of the DAG-4 shot (Catherine Snelson, personal communication). We therefore selected this multi-modal source for our study.

In detail, the DAG-4 source was a 10t chemical (nitromethane) explosion buried 51m below local ground level at 37.1146^{o}, -116.0693^{o} at NNSS with source origin time June 22, 2019

21:06:19.88 UTC. The event radiated multiple signature types that an extensive, dense set of multi-modal instruments recorded from near source (< 10m) to regional distances (> 250km). These included near-field (< 200 m) and far-field (>200 m) accelerometers, geophones, seismometers, acoustic sensors, magnetometers, and distributed acoustic sensors (DAS). The shot was also recorded with sensors from nearby seismic networks operated by the University of Nevada at Reno (UNR) (networks NN and SN) (UNR, 1971; UNR, 1992), the University of Utah (network UU), the United States Geological Survey (network US) (ASL 1990), Sandia National Laboratories (the Leo Brady Network, network LB), the Plate Boundary Observatory (network PB), and the CTBTO PrepCom's International Monitoring System (IMS) (network IM, station NVAR). These ground-truth explosive source data were used in several studies, including research on explosive source model characterization, research on P/S discriminants, and analysis for improvements to yield and depth estimates (e.g., Berg et al., 2022; Blom et al., 2020; Pyle and Walter, 2021).

Among these sensors was a sparser subset of 31 multimodal stations within ~250km of the source epicenter that were selected for building our special catalog. Our criteria for selecting these stations were that they located within a 2.33 degrees distance from the DAG-4 source epicenter, had an uptime spanning 2019-06-15 00:00:00 until 2019-06-29 23:59:59, provided no significant azimuthal gap (≤ 60 degrees), no significant distance gap (≤40 km), included reliable telemetry, and sampled both mechanical and electromagnetic waveforms (as stated above). We summarize the resulting set of candidate stations that met these requirements in Table 1, which lists the station locations and their sensing modalities which include seismic, infrasonic, and magnetometer sensors. Sensors include broadband stations (band-instrument code BH), high frequency broad band stations (HH), short period stations (SH), extremely short period (EH), and higher sample rate instruments with band-instrument codes CH (seismic) and CD (infrasound). One of our magnetometers (EM060) includes a D band label on the vertical channel and C band labels on the horizontal channels within the same sensor.

We selected this sub-network specifically to include multiple collocated, multi-modal sensors (four collocated seismic and acoustic sensors). These configurations include isolated infrasound stations deployed within a few km of seismic network stations, standalone three-component (3C) seismic sensors, a station from an IMS seismic array (NVAR), deep borehole seismic sensors that collocate with tensor strain-meters, and two magnetometers (Table 2). Depending on instrument type, location, and emplacement characteristics, these stations show varying degrees of efficacy for recording buried explosions and their background emissions (non-explosion signal sources). For example, the deep borehole stations (depths of 175km and 190km) enabled sensing of the explosion-sourced body waves without significant contamination of high frequency surface waves at far-local distances, whereas the dense seismo-acoustic network that includes collocated seismic and infrasound sensors that were deployed within 10s of km of the DAG-4 source provides sensing capability to identify ground-coupled air waves (fourth row of Table 2). Particularly unique to our data set are the magnetometer data, that provide speed-of-light sensing of the electromagnetic signal produced by the dipole source formed during the combustion process of the chemical explosion (Harlin and Nemzek, 2009; Carmichael et al., 2020). These data thereby provide a better estimate of source origin time than given by speed-of-sound seismic or acoustic waveform signals. Such data may also allow researchers to better use electromagnetic and mechanical energy partitioning as a monitoring discriminant. We excluded dense, near-source seismic sensor deployments as discussed elsewhere (Larotonda et al., 2021) since we designed our experiment to develop signal processing methods for explosion-activity monitoring, rather than to study source physics or containment mechanisms (e.g., Ford and Walter, 2013; Steedman et al., 2016).

As participants in the DAG-4 experiment, all authors of this work retained access to waveform data, but we note that some DAG-4 seismic and infrasonic waveform data were published in late 2021 to the publicly accessible Incorporated Research Institutions for Seismology (IRIS) Assembled Datasets repository, along with a data release report (Larotonda et al., 2021). An additional subset of stations are available via IRIS, including some stations in the NN, SN, UU, US, PB, LB, and IM networks. However, in both Larotonda et al., 2021 and some of the IRIS available stations, only records from the day of the DAG-4 shot and the following week (June 22-29) are available. The complete 15-day period for all stations used in this study were only available to DAG-4 participants. Thus, the complete waveform dataset will be included with this release.

We reviewed both waveform and station information for metadata quality control. This review found only that the four-element infrasound array station, RVIS, had two notable issues. First, RVIS channel metadata showed discrepancies in the element naming that appeared to change with time. Second, only two of the four components were operational (south and north directions) during the two-week window of this dataset. To accommodate the station in our processing, we separated the station into two distinct sites of RVIS and RVIN. Despite the metadata discrepancies, the waveforms were consistently of high quality and the two array units provided good azimuthal coverage to the network configuration, so RVIS and RVIN were included in our pipeline processing.

Once we completed our quality control review, we loaded station metadata and waveform header information into the National Nuclear Security Administration (NNSA) Knowledge Base Core Table schema (KbCore) tables (site, sitechan, sensor, instrument, wfdisc, affiliation) using the Python Pisces (MacCarthy, 2020) and Obspy (Beyreuther, 2010) packages. The NNSA KbCore is a modification of the CSS3.0 Database Schema (Anderson et. al., 1990) developed by NNSA to store technical information in support of nuclear explosion monitoring (Carr, 2002 and Carr, 2007). We then stored the waveforms and response files in accompanying flat files (miniSEED and KBCore .w for the former, and RESP format for the latter).

Production of Expert Analyst Catalog

We provided the fifteen-day continuous time interval database content and accompanying flat files for the seismic and infrasonic stations described above (Figure 1 and Table 1) to the expert analyst to manually build an event catalog for the period. Our goal was that the catalog would include all events that: 1) are within 340km of the DAG-4 shot and 2) triggered waveforms that could be manually observed above noise by at least three stations (seismic, infrasound, or a combination of at seismic and infrasound).

The analyst used the Analyst Review Station (ARS) with LocSAT locator and XfkDisplay (Xfk) software for phase picking and event location (tools described in Bache et. al. 1990). To construct a comprehensive event catalog, our analyst first reviewed existing events in the Advanced National Seismic System (ANSS) (see Data and Resources section) catalog that met the defined criteria as a starting point. Only the event times and locations were used from the ANSS catalog, no arrival times or associations from the ANSS catalog were used. The analyst selected each event, aligned waveforms that were visually apparent (i.e. approximately 5 signal-to-noise ratio) on each station by the Pg phase arrival, and then sorted these stations by distance to identify additional arrivals. The analyst reviewed these waveforms in multiple filter bands as necessary. An example of filter bands used for the DAG-4 event is shown in Table S1. If the analyst could manually identify arrivals recorded by at least three spatially separated (i.e. not collocated) stations, the analyst estimated phase arrival times and computed a hypocentral solution for the waveform source using the AK135 velocity model (Kenneth et al., 1995). The AK135 model was selected for two reasons: 1) to mimic an actual monitoring scenario where specific regional models may be unavailable and 2) ease of compatibility with the LocSAT software used by analyst. Location including depth, source time, and errors are calculated as part of the software output and are impacted by network geometry and density. Magnitudes were not calculated for any events in this catalog.

The analyst also identified events that were absent from the ANSS catalog. To identify such events, the analyst reviewed waveforms within eight-minute running windows, in multiple filter bands. The analyst then visually detected and phase-labeled arrivals. Infrasound phase arrivals, labeled 'I', were picked on microbarometer records and on seismic records of air-to-ground coupled arrivals. These infrasound phases were manually picked at the onset, not using peak-to-peak amplitude. Association was done manually for all event types. For infrasound signals, the 'I' phase travel-time table utilized by the International Data Center (IDC) was used to determine expected travel-times. The IDC used 270 ground-truth mine blasts and chemical explosions recorded by the IMS network to empirically establish travel times at different ranges (Brachet et. al., 2010); 330 m/s celerity for short-range tropospheric infrasound (< 1.2 degrees) and 295 m/s for intermediate range (1.2 to 20 degrees) . In the absence of array processing, the analyst judged whether an infrasound arrival was associated to an event based on the expected travel time using the travel-time tables described above and relative arrival order. Additionally, event depth was a consideration when associating infrasound arrivals to seismic events (i.e. physical mechanism for infrasound signal generation by the seismic event with a given depth). The hypocentral solutions were calculated by the same method described above for the events with an initial ANSS origin.

The analyst assigned event types by comparing event locations to known regions associated with explosion sources (i.e. mines and ordinance disposal). No discrimination software was used to differentiate between earthquake and explosion sources. If an event had multiple characteristics of an explosions, including larger Rg phases, located at a known explosion source, located at shallow depths, and all events of similar locations occurred during daytime hours, the event was identified as an explosion event type. Seismic events that could not be associated with such known regions, and that had none of the aforementioned characteristics consistent with an explosion, were left as '-' (i.e. unassigned), but are probable earthquakes. The events labeled 'eq' correlate to events assigned as earthquakes identified in the initial ANSS catalog. The earthquakes have either seismic-only arrivals or seismic and infrasound arrivals. The analyst assigned a special label, 'infrasound-only', to events that produced only infrasound arrivals, and otherwise included no obvious, known source. Additionally, there were 7 events with infrasound and seismic signals that could not be associated with any known mining blast locations or known munition disposal activities. Thus, these were assigned a label of 'seismoacoustic-unknown'.

Catalog Content

The meticulous analyst review of the two-week continuous waveform dataset resulted in a catalog of 485 events. The initial ANSS catalog contained 313 which fit our criteria; thus an additional 172 events were identified by the analyst. The catalog contains multiple event types, including the DAG-4 shot, earthquakes, explosions, infrasound-only, and seismoacoustic-unknown events (Figure 2). Of the 485 events, 295 were identified as earthquakes, 104 probable earthquakes, 25 as explosions, 7 as seismoacoustic-unknown, and 54 as infrasound-only. Most of the events are located within the network coverage and have median location errors of 7.86 km (semi-major axis) and 3.47 km (semi-minor axis). Those events located outside the network coverage have overall higher location errors with median of 11.98 km (semi-major axis) and 6.35 km (semi-minor axis). Specific event type origin location errors are shown in Table S2 and all origin error information is stored in the origerr table. Refer to Carr (2002) for a definitions of the origerr values.

The earthquakes in this dataset are located within the Great Basin in both Nevada and California, predominantly within the Walker Lane and in particular the southern portion known as the Eastern California Shear Zone (ECSZ). There are several smaller fault zones near NNSS, some within the Walker Lane and others further east, including the Rock Valley (RV) fault zone and Yucca-Frenchman (YF) shear zone (Oleary et al. 2000) likely responsible for earthquakes in this dataset. An in-depth relocation study would be needed to identify the events to the specific faulting within the region.

The DAG-4 event was in both in the ANSS catalog and in our catalog. The ground-truth location is 37.1146°, -116.0693°, with source origin time 21:06:19.88 UTC, while the analyst located the explosion at 37.11922°, -116.06573° with source origin time of 21:06:20.72 UTC. ANSS located DAG-4 at 37.112°, -116.066° with source origin time 21:06:20 UTC. Origin time and location including ground-truth for the DAG-4 shot events are included in Table S3. The ANSS solution is ~0.2 km closer to ground-truth location. Differences in location and timing between the ANSS catalog solution and our solution for DAG-4 could be attributed to several differences in processing including but not limited to 1) station selection and number of stations (i.e. we used a down-selected sub-network), 2) velocity model (regional vs global) 3) analyst subjectivity in phase picking and 4) location algorithms. Waveforms and phase arrivals for the DAG-4 shot are shown in Figure 3.

The DAG-4 event was the only known explosion with an observed infrasound phase. Records at some stations also showed pressure signals that were sourced by the passage of seismic waves that shook the infrasound sensor, before the arrival of the infrasound phase, which was excited by ground motion directly above the DAG-4 source driving a pressure pulse in the air (e.g., I20M0, Figure 3). We suspect that other events that produced observed infrasound phases and that located near mines and munition sites were explosions and were labeled as such, but ground-truth for these events is unavailable. In addition, there were seven events that were labeled seismoacoustic-unknown that occurred on June 19th that could have been explosions that had infrasound and seismic arrivals but could not be associated with any known source. The source of these events is unknown, but we speculate these could be from artillery testing. Waveforms for one of the seismoacoustic-unknown events are shown in the Figure S1 and origins are included in Table S4. Walker et. al. (2014) and Park et al. (2014) identified similar hot spots of potential infrasonic emissions associated with military regions in the area.

Ten of the 54 infrasound-only events likely came from the Army Ammunition Plant (AAP) site near the town of Hawthorne, Nevada (the "New Bomb" facility discussed in Negraru & Golden, 2017). There are 215 arrivals that are associated with these events. Because the analyst only had access to a simple distance dependent infrasonic travel-time table to locate these events, and because of the high likelihood that these events were from the AAP, the locations of these events were constrained to the published coordinates for AAP, 38.24479° and -118.64697°. Figure S2 illustrates waveforms with multiple arrivals from one of the AAP infrasound-only events. Table S5 lists origin time and location for these events.

Dataset Release Content

The dataset in this release includes the waveforms from the selected 29 seismo-acoustic stations, two magnetometer stations (Tables 1 and 2), and the station metadata. Waveforms are provided in NNSA KB Core .w format (i4) with a corresponding wfdisc table providing the header information. Station metadata sourced from IRIS and UNR are in the NNSA KB Core site, sitechan, affiliation, sensor, and instrument tables. Instrument responses are provided in RESP format.

The expert analyst catalog of 485 events, including all associated signal detections, is provided as NNSA KB Core format event, origin, origerr, arrival, and assoc tables. The 'etype' field in the origin table is used to describe the event type when known. For explosions and infrasound-only events, etype is set to 'ex' and 'infra', respectively. The etype was set to 'sa-unk' (seismoacoustic-unknown) for the seven unknown events sourced on June 19th that we described above. Additional unused fields in the arrival table were used to capture the picking filters for

DAG-4 shot. Table S6 is a key for these arrival table columns. This was only done for the DAG-4.

In addition to ASCII flatfiles for each of the tables, for those that want to load the tables into a database, we also provide a single Oracle dumpfile (.dmp) with all of the tables.

Conclusions

A goal of the geophysical explosion monitoring community is to provide the technical means to monitor the proposed CTBT for nuclear explosions of any yield, at any location on Earth. This requires developing methods that can monitor multiple geophysical signatures output by explosions to very low thresholds. Following the lead of other scientific fields that have defined standard reference models or data sets that researchers can process to define a baseline for algorithm comparison (e.g., the Utah Teapot (Dunietz, 2016), the AK135 velocity model (Kennett et al., 1995), the US Standard Atmosphere (1962)), we similarly offer a rare dataset of low yield, low magnitude events that provides a baseline reference for such algorithm comparison. Our waveform data includes records collected from seismic, acoustic, and electromagnetic stations deployed in multiple sub-networks, and our expert-analyst-built catalog includes all seismic, seismo-acoustic, and acoustic-only events that produced visible signals on three or more stations over a two-week period centered around the DAG-4 controlled explosion. This catalog includes events that locate near known tectonic regions, mining sites, and munitions disposal facilities. It also includes events that produced only infrasound signals that we speculate are sourced by artillery testing activity. We suggest that this continuous waveform dataset with comprehensively picked and labeled events and associated arrivals, is particularly useful for developing algorithms that extend the traditional, regional and teleseismic monitoring paradigm to identify smaller events using multiple modalities, recorded at near-source to near-regional distances. The data set should also prove useful for network parameter sensitivity studies that will help researchers better quantify the impact of network configurations on explosion monitoring capability.

Data and Resources

Mechanical and electromagnetic waveforms (e.g., seismograms, magnetometer signals) used in this study were collected as part of the Source Physics Experiment Phase II: Dry Alluvium Geology. Data was telemetered and stored at the non-public repository at University of Nevada, Reno during and after the experiment for two-years. Waveform and other data were released to IRIS Data Management Center under Assembled Datasets (Larotonda, 2021). This release included the day of the shot and one week of data following each chemical shot, in this case DAG-4. The ANSS catalog used as an initial reference for catalog generation can be found here: https://earthquake.usgs.gov/earthquakes/search/. The complete data set discussed in this paper (waveforms, station metadata, event catalog) titled "Multi-Modal DAG-4 Dataset" is available at IRIS Assembled Datasets here: https://ds.iris.edu/mda/23-001/. Additional figures of waveforms of the infrasound-only and seismoacoustic-unknown events and tables describing filters and origin information are included in the Supplemental Materials and referenced as Table S# and Figure S# within the main text.

Acknowledgements

The authors thank the SPE DAG-4 data providers for generating a well-characterized multi-phenomenology explosion dataset and releasing data to a public repository. The Source Physics

Experiments (SPE) would not have been possible without the support of many people from several organizations. The authors wish to express their gratitude to the National Nuclear Security Administration, Defense Nuclear Nonproliferation Research and Development, and the SPE working group, a multi-institutional and interdisciplinary group of scientists and engineers.

We also thank the developer of Pisces python package, Jonathan MacCarthy, at Los Alamos National Laboratory, for providing Obspy-compatible database software that is open-source. This research was funded by the National Nuclear Security Administration, Defense Nuclear Nonproliferation Research and Development (NNSA DNN R&D). The authors acknowledge important interdisciplinary collaboration with scientists and engineers from LANL, LLNL, MSTS, PNNL, and SNL. Portions of the work done by Lawrence Livermore National Laboratory were funded under contract by Lawrence Livermore National Security, LLC, for the U.S. Department of Energy, National Nuclear Security Administration under Contract DE-AC52-07NA27344. Portions of work done by Los Alamos National Laboratory were funded under contract by Triad National Security, LLC (LANS), operator of the Los Alamos National Laboratory under Contract No. 89233218CNA000001 with the NNSA, U.S. Department of Energy. Sandia National Laboratories is a multi-mission laboratory managed and operated by National Technology & Engineering Solutions of Sandia, LLC, a wholly owned subsidiary of Honeywell International Inc., for the U.S. Department of Energy's National Nuclear Security Administration under Contract Number DE-NA0003525.

References

Anderson, J., W. E. Farrell, K. Garcia, J. Given, H. Swanger (1990). Center for Seismic Studies Version 3 Database Schema Reference Manual, Technical Report C90-01, SAIC-90/1235, 64pp, Science Applications International Corporation.

Albuquerque Seismological Laboratory (ASL)/USGS. (1990). *United States National Seismic Network*. International Federation of Digital Seismograph Networks. https://doi.org/10.7914/SN/US

Bache, T. C., S. R. Bratt, J. Wang, R. M. Fung, C. Kobryn, and J. W. Given (1990). The Intelligent Monitoring System, *Bull. of the Seism. Soc. of Am.,* 80pp, 1833-1851.

Berg, E. M., and C. Poppeliers (2022). Inversion of Infrasound Time Series for Seismoacoustic Source Parameters Produced by a Buried Chemical Explosion at the Source Physics Experiment Phase II: Dry Alluvium Geology. *Bull. of the Seism. Soc. of Am.*, 2216–2230.

Beyreuther, M., R. Barsch, L. Krischer, T. Megies, Y. Behr, and J. Wassermann (2010). ObsPy: A Python Toolbox for Seismology, *Seismol. Res. Lett.*, *81(3),* 530-533, doi:10.1785/gssrl.81.3.530

Blom, P., A. Iezzi, and G. Euler (2020). Seismoacoustic analysis of underground explosions using the Rayleigh integral, *Geophys. J. Int*., 223, 1069-1085, doi: 10.1093/gii/ggaa363

Brachet, N., D. Brown, R. Le Bras, Y. Cansi, P. Mialle, and J. Coyne (2010). Monitoring the Earth's atmosphere with the global IMS infrasound network, *Infrasound Monitoring for Atmospheric Studies*, A. L. Pichon, E. Blanc, and A. Hauchecorne (Editors), chap. 3, pp. 77–118, Springer, Netherlands.

Carmichael, J., R. Nemzek, N. Symons, and M. Begnaud (2020). A method to fuse Multiphysics waveforms and improve predictive explosion detection: theory, experiment and performance. *Geophys. J. Int*. , 222(2), 1195-1212.

Carr, D. B. (2002). *National Nuclear Security Administration Knowledge Base Core Table Schema Document* (No. SAND2002-3055). Sandia National Laboratories, Albuquerque, NM.

Carr, D. B., J. E. Lewis, S. Ballard, E. M. Martinez, B. J. Merchant, R. Stead, M. Crown, J. Roman-Nieves, and J. Dwyer (2007). Advances in the Integration of Large Data Sets for Seismic Monitoring of Nuclear Explosions (No. SAND2007-4484C). Sandia National Laboratories, Albuquerque, NM.

Dunietz, J. (2016). The Most Important Object in Computer Graphics History Is This Teapot. *Nautilus.*

Ford, S. R., and W. R. Walter (2013). An explosion model comparison with insights from the Source Physics Experiments. *Bull. of the Seism. Soc. of Am.*, *103*(5), 2937-2945.

Harlin, J., and R. Nemzek (2009). Physical properties of conventional explosives deduced from radio frequency emissions. *Propellants, Explosives, Pyrotechnics: An International Journal Dealing with Scientific and Technological Aspects of Energetic Materials*, *34*(6), 544-550.

Kennett, B. L. N., E. R. Engdahl, and R. Buland (1995). Constraints on seismic velocities in the earth from travel times. *Geophys. J. Int*. 122:108-124.

Koper, K. D. (2020). The importance of regional seismic networks in monitoring Nuclear Test Ban Treaties. *Seismol. Res. Lett.*, *91*(2A), 573-580.

Larotonda, J. M., and M. J. Townsend (2021). Data Release Report for Source Physics Experiment Phase II: Dry Alluvium Geology Experiments (DAG-1 through DAG-4), Nevada National Security Site. *Technical Report DOE/NV/03624—1220*, 85 pages. Las Vegas, NV.

MacCarthy, J. M. (2021). Pisces: A practical seismological database library in Python. https://pypi.org/project/pisces/.

Marty, J. (2019). The IMS infrasound network: Current status and technological developments, in Infrasound Monitoring for Atmospheric Studies (Challenges in Middle Atmosphere Dynamics and Societal Benefits), Second Ed., A. L. Pichon, E. Blanc, and A. Hauchecorne (Editors), *Springer Nature*, Switzerland, p. 3-62.

NASA JPL (2013). *NASA Shuttle Radar Topography Mission Global 3 arc second* [Data set]. NASA EOSDIS Land Processes DAAC. Accessed 2023-01-20 from https://doi.org/10.5067/MEaSUREs/SRTM/SRTMGL3.003

National Research Council. (2012). The comprehensive nuclear test ban treaty: Technical issues for the United States.

Negraru, P., and P. Golden (2017). Seasonal variations of infrasonic arrivals from long-term ground truth observations in Nevada and implication for event location. *Geophys. J. Int.*, 209(1), 373-386.

O'leary, D.W. (2000). Tectonic Significance of the Rock Valley Fault Zone , Nevada Test Site.

Park, J., S. J. Arrowsmith, C. Hayward, B. W. Stump, and P. Blom (2014). Automatic infrasound detection and location of sources in the western United States. *J. Geophys. Res.*, *119*(13), 7773–7798. https://doi.org/10.1002/2013JD021084.

Pyle, M. L., and W. R. Walter (2021). Exploring the Effects of Emplacement Conditions on Explosion P/S Ratios Across Local to Regional Distances, *Seismol. Res. Lett.*, https://doi:10.1785/0220210270.

Snelson, C. M., R. E. Abbott, S. T. Broome, R. J. Mellors, H. J. Patton, A. J. Sussman, ... and W. R. Walter (2013). Chemical explosion experiments to improve nuclear test monitoring. *Eos,* *Transactions American Geophysical Union*, *94*(27), 237-239.

Steedman, D. W., Bradley, C. R., Rougier, E., and Coblentz, D. D. (2016). Phenomenology and modeling of explosion-generated shear energy for the Source Physics Experiments. *Bull. of the Seism. Soc. of Am.*, *106*(1), 42-53.

University of Nevada, Reno. (1971). *Nevada Seismic Network*. International Federation of Digital Seismograph Networks. https://doi.org/10.7914/SN/NN

University of Nevada, Reno. (1992). *Southern Great Basin Network*. International Federation of Digital Seismograph Networks. https://doi.org/10.7914/SN/SN

U.S. Standard Atmosphere. (1962). U.S. Government Printing Office, Washington, D.C., 1962, https://www.ngdc.noaa.gov/stp/space-weather/online-publications/miscellaneous/us-standard-atmosphere-1976/us-standard-atmosphere_st76-1562_noaa.pdf

Walker, K. T., R. Shelby, M. A. H. Hedlin, C. de Groot-Hedlin, and F. Vernon (2011). Western U.S. Infrasonic Catalog: Illuminating infrasonic hot spots with the USArray. *J. Geophys. Res.*, *116*(B12). https://doi.org/10.1029/2011JB008579.

Mailing Addresses

Rebecca Rodd
Lawrence Livermore National Laboratory
700 East Ave
Livermore, CA 94550
rodd2@llnl.gov

Ronald Brogan
ENSCO, Inc.
4849 N. Wickham Road
Melbourne, FL 32940
brogan.ronald@ensco.com

Joshua D Carmichael
Los Alamos National Laboratory
Bikini Atoll Rd., SM 30
Los Alamos, NM 87545
joshuac@lanl.gov

Amanda C Price
Lawrence Livermore National Laboratory
700 East Ave
Livermore, CA 94550
price54@llnl.gov

Christopher Young
Sandia National Laboratories
1515 Eubank SE
Albuquerque, NM 87123
cjyoung@sandia.gov

Tables

Table 1. The thirty-one stations centered at the DAG-4 shot location, within our search region. Each station is an assigned a modality of seismic (S), seismo-acoustic (SA), infrasound array (I), or electro-magnetic (EM) based on type of recording instruments at the station. SA (seismo-acoustic) is assigned for stations with both seismometers and acoustic sensors. Stations highlighted in yellow are historical legacy stations deployed for previous multi-physics experiments at NTS, including SPE and earlier DAG shots. Stations highlighted in green are purposed specifically for explosion monitoring.

Network	Station	Latitude	Longitude	Elevation	Distance (km)	Azimuth (degrees)	Modality
IM	NV31	38.432800	-118.155403	1509.0	234.9031	127.8797	S
LB	TPH	38.075001	-117.222504	1883.0	147.4230	135.9525	S
NN	GMN	37.300300	-117.260700	2168.0	107.7482	100.6663	S
NN	GWY	36.186001	-116.669800	1538.0	116.1974	27.3440	S
NN	PRN	37.406500	-115.051200	1464.0	95.9465	250.5754	S
NN	Q09A	38.834000	-117.181602	1703.5	214.4096	152.5397	S
NN	Q12A	39.040001	-114.829903	1625.0	239.7842	207.3526	S
NN	S11A	37.644402	-115.747200	1456.0	65.3547	205.9788	S
NN	STHB	36.645401	-116.338799	1052.0	57.3453	24.6890	S
NN	V12A	35.726601	-114.851097	1098.0	188.8304	325.0110	S
PB	B916	36.192501	-117.668503	1859.9	175.8279	53.9366	S
PB	B918	35.935699	-117.601700	1042.6	189.6001	45.9189	S
SN	AF001	37.216000	-116.161102	1637.1	13.8969	144.0469	S
SN	AF004	37.180099	-115.983398	1437.0	10.5394	226.4191	S
SN	AF005	37.189400	-116.020401	1337.2	9.3692	207.6368	S
SN	EASTD	37.115746	-115.951951	1525.1	10.4304	269.3368	SA
SN	I20M0	37.131890	-116.075617	1305.4	1.9993	163.6907	SA
SN	I20M6	37.097421	-116.062659	1269.7	1.9958	342.7982	SA
SN	L5026	37.231899	-116.115601	1808.0	13.6519	162.4563	S
SN	RV196	36.940567	-116.082591	1522.5	19.3500	3.5000	S
SN	RV339	36.810414	-116.091825	1180.3	33.8172	3.3939	S
SN	RVFF	36.728500	-115.985397	1079.0	43.4952	350.1280	S
SN	RVIS	36.705898	-115.962898	1157.8	46.3367	348.2237	I
SN	SOUF	36.798291	-115.943151	0937.9	36.8571	342.2900	S
SN	SW353	36.850486	-116.310341	1317.3	36.3271	36.1380	S
SN	SW522	37.073714	-116.109144	1312.7	5.7564	37.9654	SA
US	TPNV	36.948800	-116.249500	1600.0	24.4056	41.0135	S
UU	PSUT	38.533700	-113.854700	1999.0	250.6361	231.7507	S
UU	VRUT	37.461800	-113.856900	1874.0	199.9269	259.5593	S
SN	EM060	37.114150	-116.069079	1285.5	0.0537	338.5300	EM
SN	EM030	37.114403	-116.069174	1285.3	0.0246	332.8777	EM

Table 2. Distinct sub-networks within the complete station network. Some stations appear in multiple sub-networks. Semi-colons separate distinct sets of sub-networks. Networks are loosely defined by the physical proximity of sensors, relative to the greatest expected wavelength of a particular modality.

Sub-network description	Network-station codes
Deep seismic borehole stations (167 and 190 m depth)	PB.B916, PB.B918
Seismic array components	IM.NV31
Dense seismic networks	SN.AF001, SN.AF004, SN.AF005, SN.L5026; US.TPNV, SN.RV196, SN.RV339, SN.SOUF, SN.RVFF, SN.SW353
Seismo-acoustic arrays or networks	SN.EASTD, SN.I20M0, SN.I20M6, SN.SW522
Infrasound array components	SN.RVIS, SN.RVIN
Stand-alone three-component seismic stations	LB.TPH, NN.GMN, NN.GWY, NN.PRN, NN.Q09A, NN.Q12A, NN.S11A, NN.STHB, NN.V12A, UU.PSUT, UU.VRUT
Electromagnetic (magnetometer) stations	SN.EM030, SN.EM060
Seismic, seismo-acoustic, and magnetometer networks	SN.AF001, SN.AF004, SN.AF005, SN.EASTD, SN.I20M0, SN.I20M6, SN.L5026, SN.SW522, SN.EM030, SN.EM060

List of Figure Captions

Figure 1. Network of stations included in the data set. Seismic stations are marked as upward triangles, seismo-acoustic as inverted triangles, acoustic-only as squares, and magnetometer stations near the source are marked as diamonds. Stations are colored by network affiliation (see legend). Probable mine locations are marked as orange hexagons and the known Hawthorne Army Ammunition Plant (AAP) is marked as a black hexagon. The initial catalog from the Advanced National Seismic System (ANSS) events are marked as white circles. The rectangular inset shows a higher resolution map of the station distribution near the DAG-4 (white star) shot, where station density is higher.. The topography model used is SRTM (NASA, 2013).

Figure 2. Map of the event locations from the generated analyst catalog. Events are marked as circles, colored by event type. Unidentified events (i.e. not categorized) are red, earthquakes are orange, explosions are green, seismoacoustic-unknown are aqua, infrasound-only are blue. Stations from Figure 1 are marked as white triangles. Probable mines and Hawthorne AAP are marked as white hexagons. The rectangular inset shows a higher resolution map of the event and station distribution near the DAG-4 shot (white star), where station density is higher. The topography model used is SRTM (NASA, 2013).

.

Figure 3. Unfiltered waveforms of the DAG-4 shot recorded by three different modalities – infrasound (a), seismic (b, c, d), and electromagnetic (e, f, g, h). Dashed vertical lines indicate manual phase arrival picks, which we label and color by phase (Pg-blue, Rg-red, Lg-green, I-purple). The ground truth time of the DAG-4 event is shown as a red circle. The same time window displays seismic and infrasound waveforms. Early parts of the infrasound signal that are visible above noise on channel CDF are likely sourced by seismic ground motion at the sensor, which is visible on channels CHE, CHN and CHZ, whereas the phase marked I is sourced by the pressure pulse that is produced by ground motion above the buried explosive and that then propagates as an acoustic signal to the sensor. The electromagnetic waveforms (e-h) are zoomed-in to a shorter time-window than the infrasound and seismic (a-d). The gray box on I20M0 in (d) shows the time-window selection for the electromagnetic waveforms shown below (e-h).

A Multi-Modal Event Catalog and Waveform Data Set that Supports Explosion Monitoring from Nevada, USA

Rebecca L. Rodd[1], Ronald A. Brogan[2], Josh D. Carmichael[3], Amanda C. Price[1], Chris J. Young[4]

Supplemental Materials

Table S1: Filters used for picking DAG-4. Picking without a filter was always preferred when possible. Filter types used are not filtered, band-pass (BP), and high-pass (HP). Low-pass (LP) filters were not applied. All filter were a 3-pole Butterworth filter.

Station	Phase	Chan	FiltLow	FiltHigh	Causality	FiltType	Event-station distance (km)
I20M0	Pg	CHZ	NA	NA	NA	Not filtered	1.658
I20M0	Lg	CHN	NA	NA	NA	Not filtered	1.658
I20M0	Rg	CHZ	0.4	1.5	1	BP	1.658
I20M0	I	CDF	NA	NA	NA	Not filtered	1.658
I20M6	Pg	CHZ	NA	NA	NA	Not filtered	2.434
I20M6	Lg	CHN	0.8	NA	1	HP	2.434
I20M6	Rg	CHZ	0.4	1.5	1	BP	2.434
I20M6	I	CDF	NA	NA	NA	Not filtered	2.434
SW522	Pg	CHZ	NA	NA	NA	Not filtered	6.356
SW522	Lg	CHN	24.0	48.0	1	BP	6.356
SW522	Rg	CHZ	0.4	1.5	1	BP	6.356
AF005	Pg	CHZ	NA	NA	NA	Not filtered	8.768
AF005	Lg	CHE	3.0	6.0	1	BP	8.768
AF005	Rg	CHZ	0.4	1.5	1	BP	8.768
AF004	Pg	CHZ	NA	NA	NA	Not filtered	9.958
AF004	Lg	CHE	0.8	48.0	1	HP	9.958
AF004	Rg	CHZ	0.4	1.5	1	BP	9.958
EASTD	Pg	CHZ	NA	NA	NA	Not filtered	10.120
EASTD	Lg	CHN	3.0	6.0	1	BP	10.120
EASTD	Rg	CHZ	0.4	1.5	1	BP	10.120
L5026	Pg	CHZ	NA	NA	NA	Not filtered	13.267
L5026	Lg	CHE	2.0	5.0	1	BP	13.267
L5026	Rg	CHZ	0.4	1.5	1	BP	13.267
AF001	Pg	CHZ	NA	NA	NA	Not filtered	13.680
AF001	Rg	CHZ	0.4	1.5	1	BP	13.680
RV196	Pg	CHZ	NA	NA	NA	Not filtered	19.884
RV196	Lg	CHN	1.0	5.0	1	BP	19.884
RV196	Rg	CHZ	0.4	1.5	1	BP	19.884
TPNV	Pg	BHZ	NA	NA	NA	Not filtered	25.002
TPNV	Rg	BHZ	0.4	1.5	1	BP	25.002
RV339	Pg	CHZ	0.8	NA	1	HP	34.351
RV339	Lg	CHN	6.0	12.0	1	BP	34.351
RV339	Rg	CHZ	0.4	1.5	1	BP	34.351
SW353	Pg	CHZ	NA	NA	NA	Not filtered	36.931
SW353	Lg	CHN	NA	NA	NA	Not filtered	36.931
SW353	Rg	CHZ	0.4	1.5	1	BP	36.931
SOUF	Pg	CHZ	0.8	NA	1	HP	37.254
SOUF	Lg	CHN	6.0	12.0	1	BP	37.254
SOUF	Rg	CHZ	0.4	1.5	1	BP	37.254
RVFF	Pg	HHZ	0.8	NA	1	HP	43.950
RVFF	Lg	HHE	NA	NA	NA	Not filtered	43.950
RVFF	Rg	HHZ	0.4	1.5	1	BP	43.950
STHB	Pg	HHZ	4.0	8.0	1	BP	57.948
STHB	Lg	HHE	3.0	6.0	1	BP	57.948
STHB	Rg	HHZ	0.4	1.5	1	BP	57.948

S11A	Pg	HHZ	4.0	8.0	1	BP	64.762
S11A	Lg	HHN	4.0	8.0	1	BP	64.762
S11A	Rg	HHZ	0.5	2.0	1	BP	64.762
PRN	Pg	HHZ	4.0	8.0	1	BP	95.483
PRN	Lg	HHN	1.5	3.0	1	BP	95.483
PRN	Rg	HHZ	0.4	1.5	1	BP	95.483
GMN	Pg	HHZ	1.0	5.0	1	BP	107.970
GMN	Rg	HHN	0.4	1.5	1	BP	107.970
GWY	Pg	HHZ	0.8	NA	1	HP	116.806
GWY	Pn	HHZ	0.8	NA	1	HP	116.806
GWY	Lg	HHE	6.0	12.0	1	BP	116.806
GWY	Sn	HHE	6.0	12.0	1	BP	116.806
GWY	Rg	HHZ	0.4	1.5	1	BP	116.806
TPH	Pg	HHZ	0.8	NA	1	HP	147.286
TPH	Sn	HHN	4.0	8.0	1	BP	147.286
TPH	Rg	HHZ	0.4	1.5	1	BP	147.286
B916	Pg	EHZ	2.0	5.0	1	BP	176.394
B916	Lg	EH1	2.0	5.0	1	BP	176.394
V12A	Pg	HHZ	2.0	5.0	1	BP	189.072
V12A	Lg	HHN	2.0	5.0	1	BP	189.072
B918	Pg	EH2	3.0	6.0	1	BP	190.193
B918	Lg	EH1	0.8	3.0	1	BP	190.193
VRUT	Pg	HHZ	4.0	8.0	1	BP	199.533
VRUT	Lg	HHN	6.0	12.0	1	BP	199.533
NV31	Pn	BHZ	3.0	6.0	1	BP	234.856
NV31	Lg	BHE	2.0	4.0	1	BP	234.856
Q12A	Pg	HHZ	3.0	6.0	1	BP	239.218
Q12A	Lg	HHE	2.0	5.0	1	BP	239.218

Table S2: The median semi-major and semi-minor axis of event location error ellipse grouped by event type. Earthquakes have the smallest errors, while seismoacoustic-unknown (sa-unk) have the largest errors because the locations for AAP Hawthorne events were constrained. The location errors are determined by the LocSAT software and are largely impacted by station coverage. The location errors are populated in the origerr table in smajax and sminax fields.

Event Type	**Event Type Label**	**Median Major Axis Error (km)**	**Median Minor Axis Error (km)**
Unidentified	-	9.71	4.05
Earthquake	eq	7.95	4.04
Explosion	ex	7.65	3.76
Seismoacoustic-Unknown	sa-unk	7.34	4.66
Infrasound-Only	infra	825.06	121.43
All Events		8.86	4.29

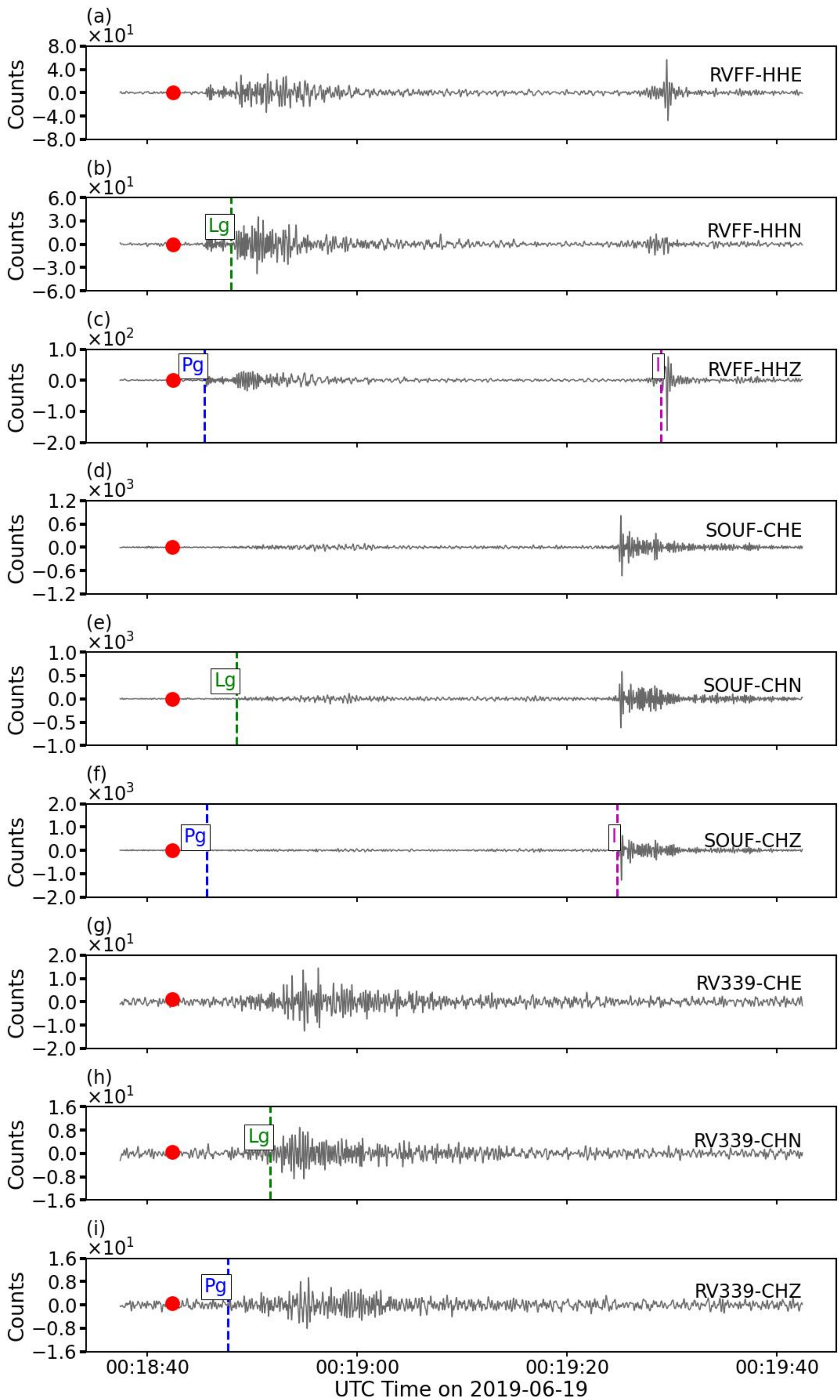
(a)
RVFF-HHE
(b)
Lg
RVFF-HHN
(c)
Pg
I
RVFF-HHZ
(d)
SOUF-CHE
(e)
Lg
SOUF-CHN
(f)
Pg
I
SOUF-CHZ
(g)
RV339-CHE
(h)
Lg
RV339-CHN
(i)
Pg
RV339-CHZ
Counts
00:18:40
00:19:00
00:19:20
00:19:40
UTC Time on 2019-06-19

Figure S1: Waveforms for a single seismoacoustic-unknown source event (orid 660) recorded on three components (E, N, Z) at the three nearest seismic stations. The infrasound arrival marks the arrival of airwave at the seismometer, which couples acoustic energy into the ground to generate seismic energy. These arrivals are labeled as an I but indicate air to ground coupled waves because they travel at the same expected speed. Arrival picks are indicated by dashed vertical lines, labeled by phase, and colored by phase: Pg-blue, Lg-green, I-purple. Phase arrivals only appear on the waveform that was picked. The origin time of the event is shown as a red circle. For example, for a three-component seismometer, arrivals were only picked on a single horizontal component, thus they are shown only on the one component.

Table S3: Catalog, ground truth, and ANSS origin information for the DAG-4 shot, including the orid key in origin table.

Origin Time	**Latitude**	**Longitude**	**Etype**	**Orid**	**Source**
06/22/2019 21:06:20.72	37.119220	-116.065730	ex	505	Catalog
06/22/2019 21:06:19.88	37.1146	-116.0692	ex	-	GT
06/22/2019 21:06:20.00	37.112	-116.066	ex	-	ANSS

Table S4: Analyst-determined origin information for the seismoacoustic-unknown source events.

Origin Time	**Latitude**	**Longitude**	**Etype**	**Orid**
06/19/2019 00:18:42	36.677486	-115.762980	sa-unk	660
06/19/2019 00:19:59	36.658874	-115.755400	sa-unk	661
06/19/2019 01:08:22	36.767532	-115.758500	sa-unk	662
06/19/2019 01:11:08	36.783598	-115.769830	sa-unk	663
06/19/2019 01:01:10	36.699484	-115.673680	sa-unk	812
06/19/2019 00:59:32	36.782645	-116.225290	sa-unk	813
06/19/2019 00:59:51	36.776072	-116.279630	sa-unk	814

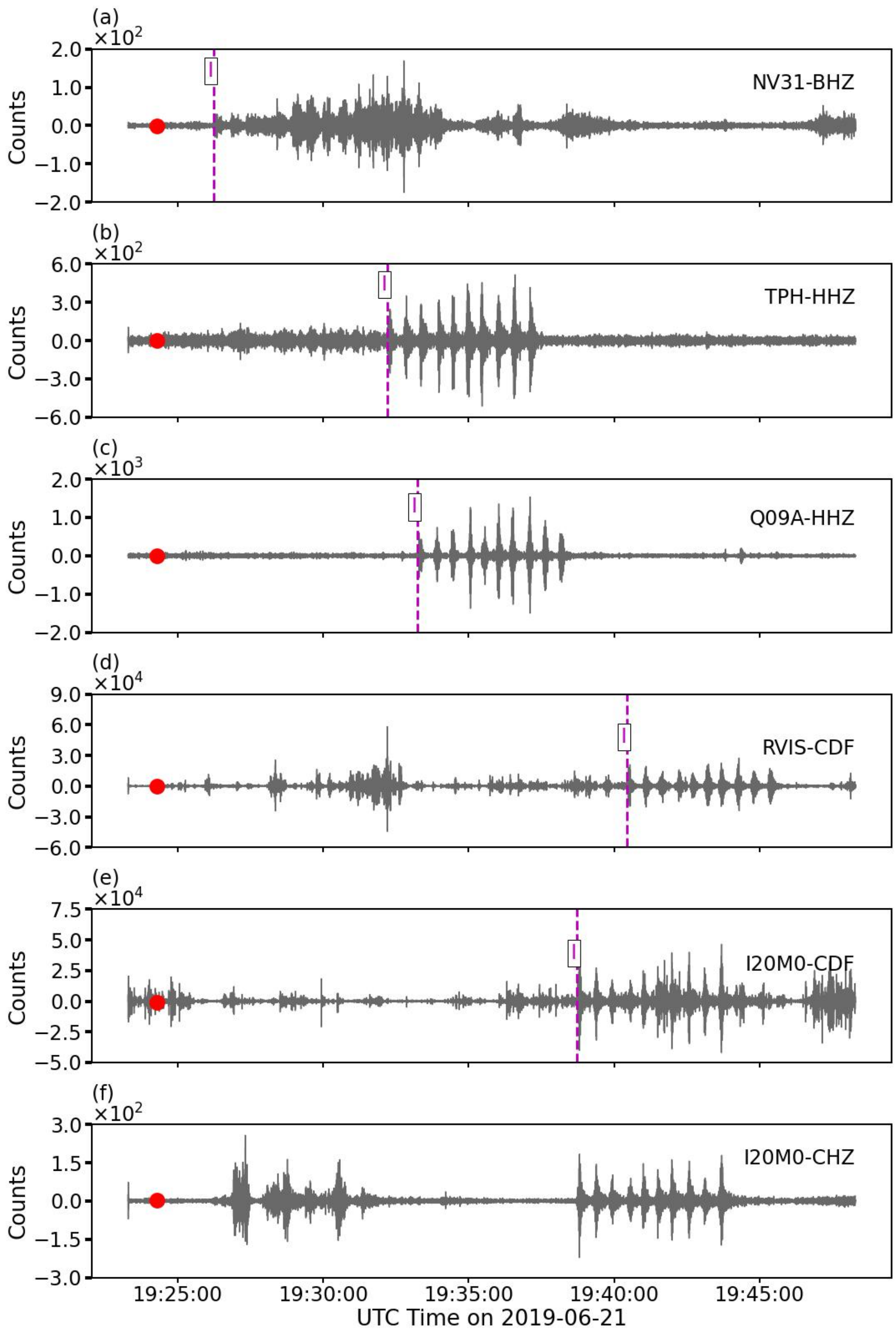
(a)
×10^2
2.0
1.0
0.0
−1.0
−2.0
Counts
I
NV31-BHZ
(b)
×10^2
6.0
3.0
0.0
−3.0
−6.0
Counts
I
TPH-HHZ
(c)
×10^3
2.0
1.0
0.0
−1.0
−2.0
Counts
I
Q09A-HHZ
(d)
×10^4
9.0
6.0
3.0
0.0
−3.0
−6.0
Counts
I
RVIS-CDF
(e)
×10^4
7.5
5.0
2.5
0.0
−2.5
−5.0
Counts
I
I20M0-CDF
(f)
×10^2
3.0
1.5
0.0
−1.5
−3.0
Counts
I20M0-CHZ
19:25:00
19:30:00
19:35:00
19:40:00
19:45:00
UTC Time on 2019-06-21

680

Figure S2: Waveforms for the Hawthorne AAP events recorded on vertical component sensors at the three nearest seismic stations and pressure sensors at the infrasound stations RVIS and I20M0. The I20M0 pressure sensor is co-located with a seismometer and the vertical waveform is included in (g) to display co-located multi-sensor types. The infrasound record in (e) measures changes in air pressure that result from the arrival of the airwave, whereas the vertical channel of seismic motion displayed (f) show local coupling of this acoustic energy into the ground, at the seismometer location. These arrivals are labeled also labeled as an I but indicate air-to-ground coupled waves because they travel at the same expected speed. The infrasound arrival picks for the first of the events (orid 572) are shown and indicated by dashed vertical purple lines and are labeled as "I". The origin time of the event is shown as a red circle.

Table S5: Origin information for the Hawthorne AAP events with source location fixed to the location of AAP site.

Origin Time	Latitude	Longitude	Etype	Orid
06/21/2019 19:23:32	38.244790	-118.645970	infra	581
06/21/2019 19:24:18	38.244790	-118.645970	infra	572
06/21/2019 19:24:52	38.244790	-118.645970	infra	584
06/21/2019 19:25:26	38.244790	-118.645970	infra	585
06/21/2019 19:26:08	38.244790	-118.645970	infra	580
06/21/2019 19:26:38	38.244790	-118.645970	infra	579
06/21/2019 19:27:07	38.244790	-118.645970	infra	577
06/21/2019 19:27:36	38.244790	-118.645970	infra	578
06/21/2019 19:28:43	38.244790	-118.645970	infra	582
06/21/2019 19:29:15	38.244790	-118.645970	infra	583

Table S6: Key for altered arrival table columns in DAG-4 where each column represents a different filter parameter.

Arrival Table Column	Attribute
ema	Filter low-cut Hz
rect	Filter high-cut Hz
clip	Filter causality (0=unfiltered, 1=causal,2=non-causal)
fm	Filter type (Bandpass, Highpass, Lowpass, Unfiltered)